Development 139, 2955-2965 (2012) doi:10.1242/dev.077982

Absence of Dpy19l2, a new inner nuclear membrane protein, causes globozoospermia in mice by preventing the anchoring of the acrosome to the nucleus

Virginie Pierre[1,2], Guillaume Martinez[1,2,3], Charles Coutton[1,2,4], Julie Delaroche[1,5], Sandra Yassine[1,2], Caroline Novella[1,2], Karin Pernet-Gallay[1,5], Sylviane Hennebicq[1,2,3], Pierre F. Ray[1,2,6,*] and Christophe Arnoult[1,2,*,‡]

SUMMARY

Sperm-head elongation and acrosome formation, which take place during the last stages of spermatogenesis, are essential to produce competent spermatozoa that are able to cross the oocyte zona pellucida and to achieve fertilization. During acrosome biogenesis, acrosome attachment and spreading over the nucleus are still poorly understood and to date no proteins have been described to link the acrosome to the nucleus. We recently demonstrated that a deletion of *DPY19L2*, a gene coding for an uncharacterized protein, was responsible for a majority of cases of type I globozoospermia, a rare cause of male infertility that is characterized by the exclusive production of round-headed acrosomeless spermatozoa. Here, using *Dpy19l2* knockout mice, we describe the cellular function of the Dpy19l2 protein. We demonstrate that the protein is expressed predominantly in spermatids with a very specific localization restricted to the inner nuclear membrane facing the acrosomal vesicle. We show that the absence of Dpy19l2 leads to the destabilization of both the nuclear dense lamina (NDL) and the junction between the acroplaxome and the nuclear envelope. Consequently, the acrosome and the manchette fail to be linked to the nucleus leading to the disruption of vesicular trafficking, failure of sperm nuclear shaping and eventually to the elimination of the unbound acrosomal vesicle. Finally, we show for the first time that Dpy19l3 proteins are also located in the inner nuclear envelope, therefore implying that the Dpy19 proteins constitute a new family of structural transmembrane proteins of the nuclear envelope.

KEY WORDS: Dpy19l2, Acrosome biogenesis, Globozoospermia, Nuclear envelope, Nuclear lamina, Spermiogenesis, Mouse

INTRODUCTION

Spermatozoon is doubtless one of the most specialized cells in mammals and the description and understanding of the molecular aspects of spermiogenesis represents a very challenging task. The acrosome, a giant vesicle of secretion tightly bound to the nucleus via the acroplaxome (a network of proteins including keratin 5 and β-actin) (Kierszenbaum et al., 2003), is a highly specialized organelle found only in sperm. The molecular basis of acrosome biogenesis, and particularly its attachment and spreading over the nucleus, are poorly understood at molecular level; to date, there has been no report of any protein of the nuclear envelope (NE) anchoring the acroplaxome to the nuclear dense lamina (NDL) (Kierszenbaum et al., 2011). Knockout animal models presenting with spermiogenesis defects are interesting tools with which to characterize new actors of spermatid differentiation. Among teratozoospermia, globozoospermia is characterized by the production of round-headed acrosomeless spermatozoa and mouse strains presenting with such a defect represent very valuable models to decipher acrosome biogenesis. Globozoospermia was first described in human (Schirren et al., 1971), and familial cases rapidly pointed to a genetic pathogenesis. In recent years *SPATA16* (Dam et al., 2007b) and *DPY19L2* were described to be involved in globozoospermia (Harbuz et al., 2011; Koscinski et al., 2011). SPATA16 located in the Golgi apparatus is likely to be involved in vesicular trafficking necessary for acrosome biogenesis but its precise function remains uncharacterized (Lu et al., 2006; Xu et al., 2003). *DPY19L2* is a testis-specific member of an uncharacterized gene family, including four genes in mammals: *DPY19L1* to *L4* (Carson et al., 2006). The inactivation of *DPY19*, the ortholog of *DPY19L2* in *C. elegans*, was showed to block neuroblasts migration during the worm organogenesis (Honigberg and Kenyon, 2000). Its cellular localization and its physiological role have, however, remained elusive so far. We therefore decided to study *Dpy19l2* knockout mice (*Dpy19l2*$^{-/-}$) to unravel the function of Dpy19l2. In mice, a total of eight genes has been described to trigger globozoospermia. The first group of four proteins – Pick1 (Xiao et al., 2009), Gopc (Yao et al., 2002), Vps54 (Paiardi et al., 2011) and Hrb (Kang-Decker et al., 2001), as SPATA16 – controls Golgi vesicles fusion necessary for acrosome formation. The second set of globozoospermia-inducing proteins comprises Zpbp1 (Lin et al., 2007), Ck2α′ (Xu et al., 1999), Hsp90b1 (Audouard and Christians, 2011) and Gba2 (Yildiz et al., 2006), which have more diverse cellular localizations and functions: Zpbp1 and Ck2α′ are proteins of the acrosomal matrix, whereas Hsp90b1 is expressed in the reticulum and Gba2 is expressed in both germ and Sertoli cells. Table S1 in the supplementary material summarizes the main characteristics of these mouse mutants. None perfectly mirrors the round-shaped acrosomeless spermatozoa observed in human type 1 globozoospermia, suggesting that Dpy19l2 has an original cellular function during spermiogenesis.

[1]Université Joseph Fourier, Grenoble F-38000, France. [2]Equipe 'Génétique, Infertilité et Thérapeutiques' Laboratoire AGIM, CNRS FRE3405, La Tronche F-38700, France. [3]CHU de Grenoble, Centre d'AMP-CECOS, BP217, Grenoble cedex 9 F-38043, France. [4]CHU de Grenoble, UF de Génétique Chromosomique, Grenoble F-38000, France. [5]Grenoble Institut des Neurosciences, INSERM U.836, Grenoble F-38000, France. [6]CHU de Grenoble, UF de Biochimie et Génétique Moléculaire, Grenoble F-38000, France.

*Joint co-authors
‡Author for correspondence (christophe.arnoult@ujf-grenoble.fr)

Accepted 23 May 2012

The goal of this study was to characterize the cellular location of Dpy19l2 and to elucidate its function during spermiogenesis. We demonstrate here that Dpy19l2 is a transmembrane protein expressed specifically in spermatids and that it is localized only in the inner nuclear membrane (INM) of the nucleus facing the acrosome. In *Dpy19l2*$^{-/-}$ males, we observed a progressive fragmentation of the NDL facing the acroplaxome, which was concomitant with a detachment of the acrosome. We propose that Dpy19l2 participates in the anchoring of the acrosome to the nucleus, bridging the NE to both the NDL and the acroplaxome. Our results therefore indicate that in mouse *Dpy19l2*-induced globozoospermia is due to a default in the attachment of the NE to the acroplaxome and to the NDL. Such a defect has never been described in any species so far. We furthermore showed that DPY19 proteins constitute a new family of membrane nuclear proteins, therefore opening a new field of research in proteins involved in nucleus-cytoplasm interactions.

MATERIALS AND METHODS

Biological preparations

Human

Sperm were obtained from the fertility department of Grenoble Hospital (France), following approval by the ethical committee and informed consent from the patient.

Animals

All animal procedures were run according to the French guidelines on the use of animals in scientific investigations with the approval of the local Ethical Committee. *Dpy19l2*$^{-/-}$ mice were obtained from Mutant Mouse Regional Resource Center (University of California, Davis, CA, USA). Although gene knockout had been checked by PCR/Southern (http://mmrrc.mousebiology.org/doc/di_032274PCR_Protocol.pdf), we confirmed by RT-PCR that Dpy19l2 transcripts were absent (not shown).

Spermatogenic cells dissociation

Detunicated testes were incubated in 5 ml of collagenase solution (1 mg/ml in EKRB) for 30 minutes at room temperature. The dispersed seminiferous tubules were washed with PBS and cut thinly. Cells were dissociated by gently pipetting and pelleted by centrifugation at 500 ***g*** for 10 minutes. Cells were suspended in 1 ml PBS and fixed in 4% PFA solution, washed with PBS and finally layered onto polylysine-coated slides.

For EM experiments, cell suspensions were loaded into a sedimentation chamber according to procedures developed for murine spermatogenic cells for velocity sedimentation under unit gravity separation (Romrell et al., 1976).

Sperm analysis

Sperm was displayed over a slide and dried at room temperature, then fixed in Ether/Ethanol 1:1 for Harris-Schorr stain or in methanol for lectin staining [10 μg/ml PSA-Rhodamin (Vector Laboratories)].

Antibodies

Mouse sperm protein sp56 monoclonal antibodies were from QED Bioscience; lamin B1 antibodies were from Abcam (Ab16048); acetyl histone H4 antibodies (06-598) were from Millipore; and DDK-tag antibodies were from Origene. Dpy19l2 antibodies were produced in rabbit as polyclonal antibodies raised against RSKLREGSSDRPQSSC and CTGQARRRWSAATMEP peptides corresponding to amino acids 6-21 and 21-36 of the N terminus of mouse Dpy19l2.

Histology and immunohistochemistry

Testes were fixed for 24 hours in 4% PFA. Tissue was dehydrated in a graded ethanol series, embedded in paraffin and sectioned at 4 μm onto slides. For histology studies, sections were stained via automated slides stainer (Leica Autostainer XL V2.2). For immunohistochemistry, heat antigen retrieval was performed by boiling slides immersed in 0.01 M sodium citrate buffer, 0.05% Tween 20 (pH 6.0) for ~25 min. Incubation with primary antibodies was performed overnight at 4°C in PBS with 2% goat serum, 1% bovine serum albumin, 0.1% Triton X-100. Slides were then washed and incubated with secondary antibodies for 1 hour at room temperature and counterstained with Hoechst. Images were taken by confocal microscopy (Zeiss LSM 710) and processed using Zen 2009.

Electron microscopy (EM)

Immunogold labeling

Purified spermatids were fixed in 0.1 M phosphate buffer (pH 7.3) containing 2% PFA and 0.2% glutaraldehyde. Cells were then washed twice in 0.1 M phosphate buffer and once in 0.1 M (pH 7.2) phosphate buffer/50 mM glycine before being centrifuged and embedded in 10% gelatin diluted in the same buffer at 37°C. After solidification on ice, this cell pellet was incubated for 4 hours in 2.3 M sucrose and frozen in liquid nitrogen. Cryosections of these samples were made at –120°C using an ultra-cryo-microtome (Leica-Reichert) and retrieved with a 1:1 solution of 2.3 M sucrose and 2% methylcellulose according to Liou et al. (Liou et al., 1996). For labeling, cryosections were first incubated with primary α-Dpy19l2 antibody and revealed with protein A-gold conjugated (CMC, Utrecht, The Netherlands).

Morphological analysis

Spermatids were fixed with 2.5% glutaraldehyde in 0.1 M cacodylate buffer (pH 7.4). Cells were then embedded in 10% gelatin diluted in 0.1 M cacodylate. After solidification, samples were post fixed with 1% osmium tetroxide and 0.1 M cacodylate (pH 7.2) for 1 h at 4°C. After washing, cells were further stained with 1% uranile acetate (pH 4) for 1 hour at 4°C before being dehydrated through graded alcohol and infiltrated with a mix of 1/1 epon/alcohol (100%) for 1 hour and several baths of fresh epon (Sigma) for 3 hours. Finally, samples were included in a capsule full of resin that was let to polymerize for 72 hours at 60°C. Ultra thin sections of the cell samples were cut with an ultramicrotome (Leica), sections were post-stained with 5% uranile acetate and 0.4% lead citrate and observed in an electron microscope at 80 kV (JEOL 1200EX).

Cell culture, transfection and nuclei preparation

HEK-293 and NH3T3 cells were grown in Dulbecco's Modified Eagle's Medium supplemented with 10% FBS (Invitrogen, France) and transiently transfected with pEGFP and human orthologs of Cter-tGFP-tagged-DPY19L2, Cter-DDK-tagged DPY19L3 and Cter-DDK-tagged SUN5 containing pCMV6 plasmids (from Origene, Rockville, MD, US) alone or in combination, using Lipofectamine 2000 Transfection Reagent (Invitrogen) according to the manufacturer's instructions. Two days after transfection, transfected cells were fixed with 4% PFA before immunochemistry experiments.

Nuclei were prepared in cold hypotonic buffer and obtained after loose dounce homogenizer according to Zhong et al. (Zhong et al., 2010). Nuclei were pelleted at 2000 ***g*** for 20 minutes at 4°C and fixed in 4% PFA.

Statistical analyses

Statistical analyses were performed with SigmaPlot. A *t*-test was used to compare wild-type and *Dpy19l2*$^{-/-}$ samples. Data presented represent mean ± s.e.m. Two-tailed statistical tests with $P \leq 0.05$ were considered as statistically significant.

RESULTS

Dpy19l2$^{-/-}$ mice are sterile and sperm present a round shaped head with multiple defects

Dpy19l2$^{-/-}$ mice were very succinctly described as infertile in a mouse knockout library established for transmembrane proteins (Tang et al., 2010). This was consistent with our result concerning the impact of *DPY19L2* deletion in human fertility (Harbuz et al., 2011). Here, we performed a much finer reproductive phenotyping. First, *Dpy19l2*$^{-/-}$ males were sterile, whereas *Dpy19l2*$^{+/-}$ males were perfectly fertile (Fig. 1A). The only anatomical defect observed was a decrease of the weight and size of the *Dpy19l2*$^{-/-}$ testis in comparison with wild-type male siblings (Fig. 1B,C). In testis sections stained with Eosin/Hematoxylin, the lumens of

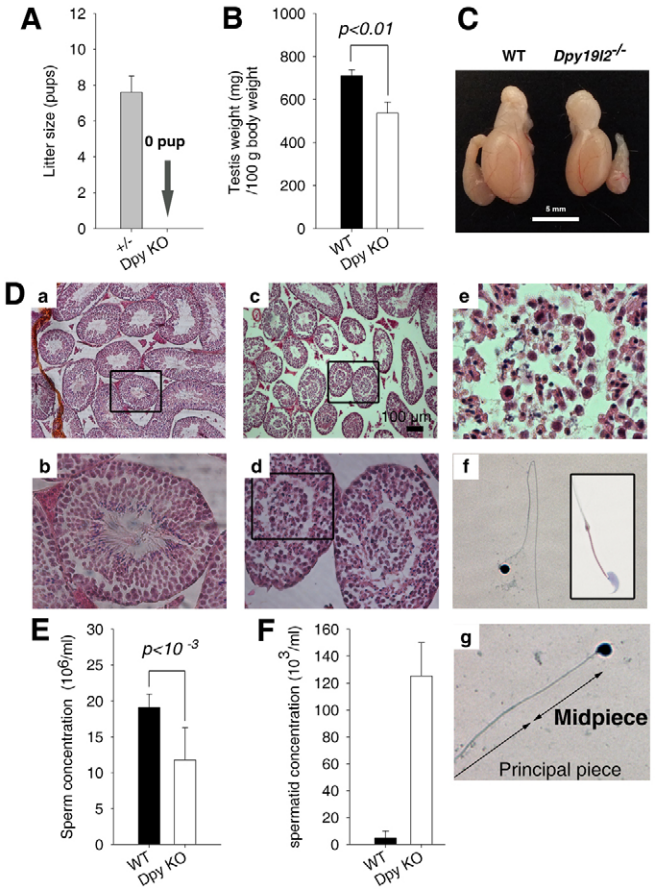

Fig. 1. Spermiogenesis is abnormal in *Dpy19l2*$^{-/-}$ males and they are sterile. (**A**) No pup was born when *Dpy19l2*$^{-/-}$ males were mated with wild-type females (n=10). (**B**) *Dpy19l2*$^{-/-}$ males had a smaller testes than wild-type males (n=6). (**C**) Typical size of wild-type and *Dpy19l2*$^{-/-}$ testes of male siblings. Scale bar: 5 mm. (**D**) Contrary to what is observed in wild-type testis (sections stained with Eosin-Hematoxylin) (a) (b is the enlargement of the black box in a), a mass of cells characterized by different sizes and different condensation states of their nucleus is present in some lumens of *Dpy19l2*$^{-/-}$ tubules (c) (d is the enlargement of the black box in c; e is the enlargement of the black box in d). (f,g) Most of the spermatozoa (>70%) presented with a round-shaped head. Inset shows a wild-type mouse sperm. (**E**) *Dpy19l2*$^{-/-}$ males presented a smaller concentration of epididymal sperm than did wild-type males (n=4). (**F**) In sperm obtained from *Dpy19l2*$^{-/-}$ epididymides extracts, large cells similar to those observed in the tubule sections were present at a concentration of around 1.25×10^5 cells. These cells were not observed in wild-type epididymides extracts (n=4). Data are mean±s.e.m.

tubules from wild-type males were large and many flagella were observed (Fig. 1Da,Db). By comparison, the structure of the tubules from a *Dpy19l2*$^{-/-}$ littermate was clearly disorganized: the most striking difference was the presence of numerous large cells in some lumens (Fig. 1Dc,Dd). When stained with Hematoxylin, the nucleus of these cells appeared dark blue (Fig. 1De), indicating that these cells are probably male germ cells. Spermiogenesis arrest usually leads to spermatid apoptosis, which could explain the observed decreased testicular weight (Romero et al., 2011; Xiao et al., 2009). Thus, we measured the number of apoptotic cells in testis slices with a TUNEL test, but we observed no apoptotic cells from controls nor *Dpy19l2*$^{-/-}$ males tubules sections (data not shown). In epididymis, *Dpy19l2*$^{-/-}$ sperm were globozoospermic with the canonical round-shaped sperm heads (Fig. 1Df,Dg). The small decrease of testis size was associated with a decrease in sperm concentration in the cauda epididymides, which was almost halved ($19\times10^6\pm3$/ml and $11\times10^6\pm9$/ml in wild-type and *Dpy19l2*$^{-/-}$ sperm, respectively) (Fig. 1E). Interestingly, large cells, which correspond to the aborted spermatids observed in the lumens of the tubules, were present among epidydimal sperm at a concentration of ~1.25×10^5 per ml (Fig. 1F). This type of cell was not present in wild-type sperm.

At the cellular level, the morphological aspect of spermatozoa from *DPY19L2* homozygously deleted men and knockout mice was remarkably similar (supplementary material Fig. S1B), with round-shaped sperm heads. Harris-Shorr stained spermatozoa presented various morphological defects. First ~99% of the sperm population presented an important defect in the midpiece, with ~70% sperm presenting a complete absence of the mitochondrial sheath (Fig. 1Dg; supplementary material Fig. S1A,B) and 29% a partial and disorganized sheath (supplementary material Fig. S1C,D). Defects were also observed in the principal piece with ~20% of sperm presenting coiled tails (supplementary material Fig. S1E,F) and ~9% presenting several flagella (supplementary material Fig. S1G,H). Finally, ~1% of sperm presented incomplete individualization between spermatozoa (supplementary material Fig. S1I,J).

Dpy19l2 is a polarized protein facing acrosome

In order to understand why the absence of Dpy19l2 leads to the formation of round headed acrosomeless spermatozoa, we first determined the cellular location of the protein by performing immunohistochemistry experiments with an antibody raised against Dpy19l2. In wild-type tubule sections, a strong polarized staining was observed in round spermatids (Fig. 2A). However, this staining was absent in *Dpy19l2*$^{-/-}$ spermatids (Fig. 2B). We also performed staining with another antibody targeting a different peptide of the N-ter and an identical staining was observed (data not shown). Finally, triple staining with Dpy19l2 antibody, sp56 antibody [to visualize the acrosome: sp56 is a protein of the acrosomal matrix in spermatids and incapacitated sperm (Kim et al., 2001)] and Hoechst was performed to demonstrate the antigenicity of *Dpy19l2*$^{-/-}$ sections (Fig. 2C,D). Altogether, these results demonstrate the specificity of the staining.

In order to obtain a more accurate localization of the protein in the different germ cell types, testis cells were fractionated by sedimentation in a BSA gradient and triple stained (α-Dpy19l2, α-sp56 and Hoechst). No specific staining was observed in pachytene spermatocytes (data not shown). However, in round spermatids, Dpy19l2 staining is organized as a cap over the nucleus facing the acrosome (Fig. 2E-G). In condensed spermatids, Dpy19l2 covers the whole acrosomal area, including the equatorial and dorsal segments, contrary to sp56, which at this stage is restricted to the dorsal segment of the acrosome (Fig. 2H-J). Interestingly, we did not observe any Dpy19l2 staining in epididymal sperms, suggesting that the protein had been remodeled at this stage (supplementary material Fig. S2A-F). This result confirms our previous results obtained by western blot showing the absence of Dpy19l2 protein in human and mouse mature sperm (Harbuz et al., 2011). Lamina-associated polypeptide 2 (LAP2), lamin B1 and B3 are also remodeled during epidymal transit and are absent in mature sperm cells (Alsheimer et al., 1998; Schutz et al., 2005). The remodeling of NE is probably related to the deep modifications of the nucleus during epidydimal transit.

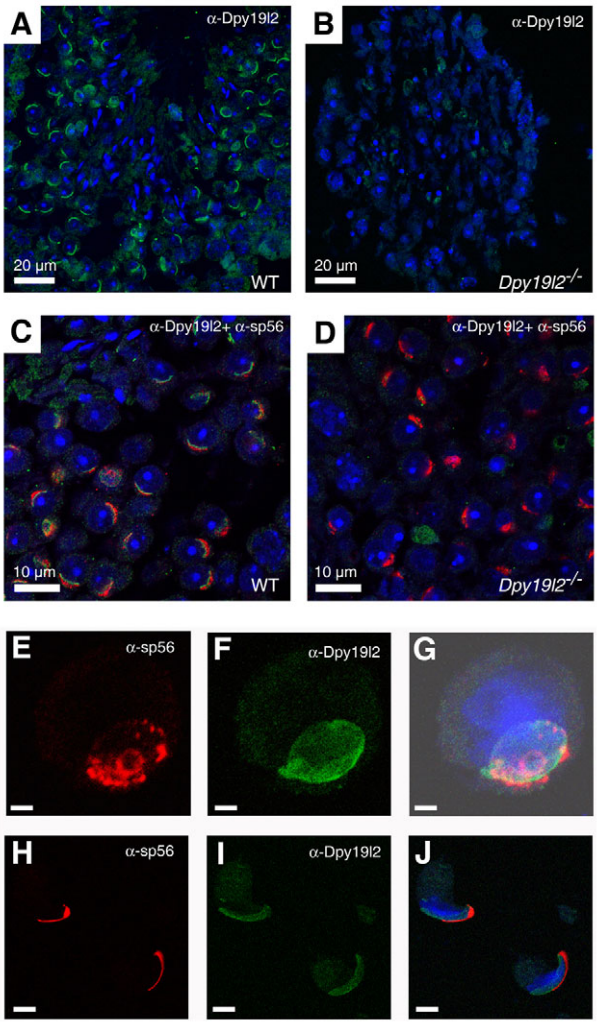

Fig. 2. Immunostaining of Dpy19l2 shows its acrosomal localization in wild-type spermatids. (**A**) Wild-type tubule sections stained with an antibody raised against Dpy19l2 (α-Dpy19l2) and counterstained with Hoechst to show the nucleus (blue). In round spermatids, the antibody recognized a structure located in the acrosomal cap area (green). (**B**) The same antibody did not recognize any acrosomal structure in tubule sections from *Dpy19l2*$^{-/-}$ testis. (**C**,**D**) Comparison of wild-type and *Dpy19l2*$^{-/-}$ tubule sections stained with α-Dpy19l2 (green), α-sp56 antibodies (to show the acrosomal matrix; red) and Hoechst (blue). (**E-J**) An isolated round spermatid, at step 5 of spermiogenesis (cap phase) (E-G) and condensed spermatids at step 12 of spermiogenesis (H-J), were labeled with α-sp56, α-Dpy19l2 and Hoechst. (E,H) Sp56 staining. (F,I) Dpy19l2 staining. (G,J) Overlay. Scale bars: 20 μm in A,B; 10 μm in C,D; 1 μm in E-G; 0.5 μm in H-J.

Dpy19l2 is a protein of the inner nuclear membrane

The localization of Dpy19l2 identified above may correspond to different subcellular structures such as the inner acrosomal membrane or the NE. To determine the localization of Dpy19l2, we first transfected, alone or in combination, one member of the DPY19L family, DPY19L2 or DPY19L3, and SUN5 (also known as SPAG4L), a member of the SUN family, in HEK and NH3T3 cells. DPY19L2 was tagged with GFP, and DPY19L3 and SUN5 were tagged with DDK. We chose SUN5 as a marker of the inner nuclear membrane (INM) because it was recently demonstrated that SUN5 is positioned in round spermatids in the NE facing the acrosomal vesicle (Frohnert et al., 2011).

First, as expected for a SUN protein, SUN5 immunostaining formed a nuclear rim-like pattern when transfected alone (Fig. 3A,A′). DPY19L2-GFP fluorescence was also in the peri-nuclear area but the staining was more discontinuous and more clustered around the nuclear rim (Fig. 3B-B″). Because GFP-tag may modify the localization of a tagged protein, we also transfected DPY19L3-DDK, a different member of the DPY19L family. DPY19L3 immunostaining formed a nuclear rim-like pattern very similar to SUN5 immunostaining (supplementary material Fig. S3A). The immunostaining remained attached to isolated nuclei obtained by dounce cell lysis after cell swelling in hypoosmostic solution (supplementary material Fig. S3B). These results suggest that NE is the target organelle for all members of the DPY19L family. When DPY19L2 and SUN5 were co-transfected, DPY19L2-GFP staining partially colocalized with SUN5 staining, but with a striking spatial organization where DPY19L2-GFP fluorescence was located in a more internal nuclear location than SUN5-DDK immunostaining (Fig. 3C,D). Because HEK cells present a small cytoplasmic compartment that makes it difficult to focus only on the nuclear area, double staining were also performed on isolated nuclei. Isolated nuclei presenting NE swelling, evidenced by the presence of a space between SUN5 staining and DNA staining, presented a similar pattern of staining [isolated nuclei prepared in hypo-osmotic solution present with partial NE swelling (Dahl et al., 2004)]: in these nuclei, DPY19L2-GFP fluorescence was also in a more internal nuclear location than SUN5 immunostaining (Fig. 3E-G). Both tags were located at the C terminus of the proteins. The C terminus of SUN proteins is located in the NE lumen (Hodzic et al., 2004) and the fact that GFP staining was in a more internal nuclear location, is incompatible with a localization of DPY19L2 in the outer nuclear membrane (ONM) and thus demonstrates the INM location of DPY19L2 in cell lines. Moreover, this result suggests that the C terminus of DPY19L2 is located in the nucleoplasm. To confirm the nucleoplasmic location of the C terminus of DPY19L proteins, we compared SUN5/DPY19L3 immunostainings obtained with or without permeabilization of isolated nuclei. Similar immunostaining was observed on non-permeabilized or permeabilized isolated nuclei from SUN5-DDK transfected HEK cells with antibodies against SUN5-DDK, suggesting that ONM was partially damaged by the nuclei isolation process (supplementary material Fig. S3Ca,Cb). However, isolated nuclei from DPY19L3-DDK transfected HEK cells were immunostained only after Triton-X100 permeabilization (supplementary material Fig. S3Cc,Cd). The results of these last experiments were in accordance with a nucleoplasmic localization of the C terminus of DPY19L proteins. To confirm that Dpy19l2 is located in the INM in spermatids, we then performed immunogold labeling with EM. In round spermatids at step 5-6 of spermiogenesis, immunogold particles were restricted and positioned all along the bridging structure of the acrosome, corresponding to the NDL, the NE and the acroplaxome (Fig. 4A,B; supplementary material Fig. S4A-D). In step 9, we observed a similar immunogold staining (supplementary material Fig. S4D). This first set of immunogold labeling results unequivocally demonstrated that Dpy19l2 is also located in the NE in spermatids.

The antibody targets the N-terminal domain of this transmembrane protein (amino acids 6-21) and thus could be located (1) on the cytosolic face of the ONM, (2) in the lumen of the NE or (3) in the nucleoplasm. As mentioned in the

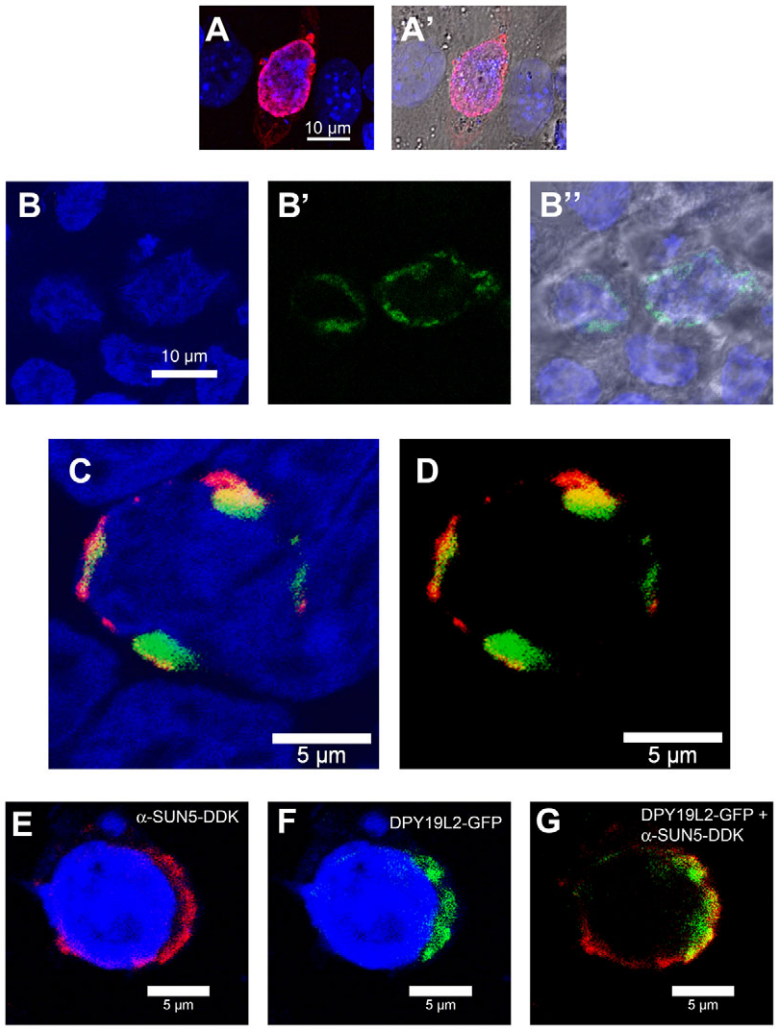

Fig. 3. DPY19L2 and SUN5 are located in the nuclear envelope when heterologously expressed in cell lines. (**A**,**A'**) NH3T3 cells were transfected with pCMV6-SUN5-DDK and immunofluorescence staining observed after Hoechst nuclei counterstaining. (A) Overlay of Hoechst and SUN5-DDK immunostaining and (A') overlay of Hoechst, SUN5-DDK immunostaining and phase contrast. (**B-B''**) HEK cells were transfected with pCMV6-DPY19L2-GFP and fluorescence of GFP measured by confocal microscopy. (**C-G**) SUN5-DDK immunostaining partially overlaps with DPY19L2-GFP: the C terminus of DPY19L2-GFP is located closer to the nucleus than the C terminus of SUN5. HEK cells were transfected with both DPY19L2-GFP and SUN5-DDK plasmids. Double transfected cells were analyzed with confocal microscopy after nuclei counterstaining with Hoechst. (C,D) DPY19L2 fluorescence (green) was located in a more internal nuclear location than SUN5 staining (red), showing that the C terminus of DPY19L2-GFP is located closer to the nucleus than the C terminus of SUN5. The yellow corresponds to SUN5-DPY19L2 colocalization. (E-G) Isolated nuclei of double transfected HEK cells presented a DPY19L2-GFP fluorescence (green) in a more internal nuclear localization than SUN5 immunostaining (red) at the nuclear envelope. Scale bars: 10 μm in A-B''; 5 μm in C-G.

literature, the observed position of the gold particles did not allow the direct determination of the precise localization of the antigenic site because gold particles fall in a 80 nm diameter circle around the antigenic site because of the lengths of IgG [20 nm × 2 (IgG × 2)=40 nm]. In order to better characterize the localization of the N-ter, we first measured the frequency of the gold particle positioning in relation to different sites: (1) the NDL, (2) the INM and ONM, and (3) the acroplaxome (Fig. 4C). Gold particles were most frequently located in the NDL area (Fig. 4D). Second, we measured the shortest distance from the centre of the gold particle to the line splitting both nuclear membranes (Fig. 4E): measures were counted positively when heading towards the nucleus and negatively when heading toward the acrosome. As the distribution of the gold particles in its circle is random, the median of the sample should be 0 for a location in the NE lumen, around –10 nm if the epitope is located on the cytosolic side of the ONM, and +10 nm for a location in the nucleoplasm. A box-plot corresponding to the numerical values of the distances of 52 gold particles is showed in Fig. 4F and a median of +14.36 nm was determined. This result strongly suggests that the N-ter of Dpy19l2 is located in the nucleoplasm in mouse spermatids. All together, transfection and EM results demonstrate that DPY19L2 is localized in the INM of round spermatids, with both N-and C-ter in the nucleoplasm.

Caudal descent and acrosome spreading are defective in the absence of Dpy19l2

In order to understand the role of Dpy19l2 in acrosome biogenesis, ultrastructural studies of acrosome formation were performed by EM on spermatogenic cells from *Dpy19l2*$^{-/-}$ males sorted by sedimentation velocity (Barcellona and Meistrich, 1977; Romrell et al., 1976). First, initial acrosome binding at step 3 was not disrupted and we observed no differences in the acrosomal junctional structures between wild-type and *Dpy19l2*$^{-/-}$ mice (Fig. 5A,B). However, the acrosomal matrix, which binds tightly to the acroplaxome at this step (Fig. 5A), had an ectopic localization, binding to the outer acrosomal membrane (Fig. 5B,D, black arrows). Acrosome of *Dpy19l2*$^{-/-}$ sperm in step 4 of the spermiogenesis had a similar volume and extension compared with wild-type acrosomes (Fig. 5C,D). However, new defects appeared, including the presence of numerous vacuoles in the acrosome (Fig. 5D, white arrows). During the next steps, the caudal descent of the acrosome was clearly hampered. Numerous spermatids were blocked at stage 5 (Fig. 6). The extension of the NDL was not observed (Fig. 6B,C), leading to a complete block of bilateral acrosome extension. Instead of spreading over the nucleus, the acrosome swelled (Fig. 6C). This bloating is correlated with an increase in the size and the number of the vacuoles. This vacuolization probably corresponds to acrosomal membrane invagination caused by the continuing flux of Golgi-derived

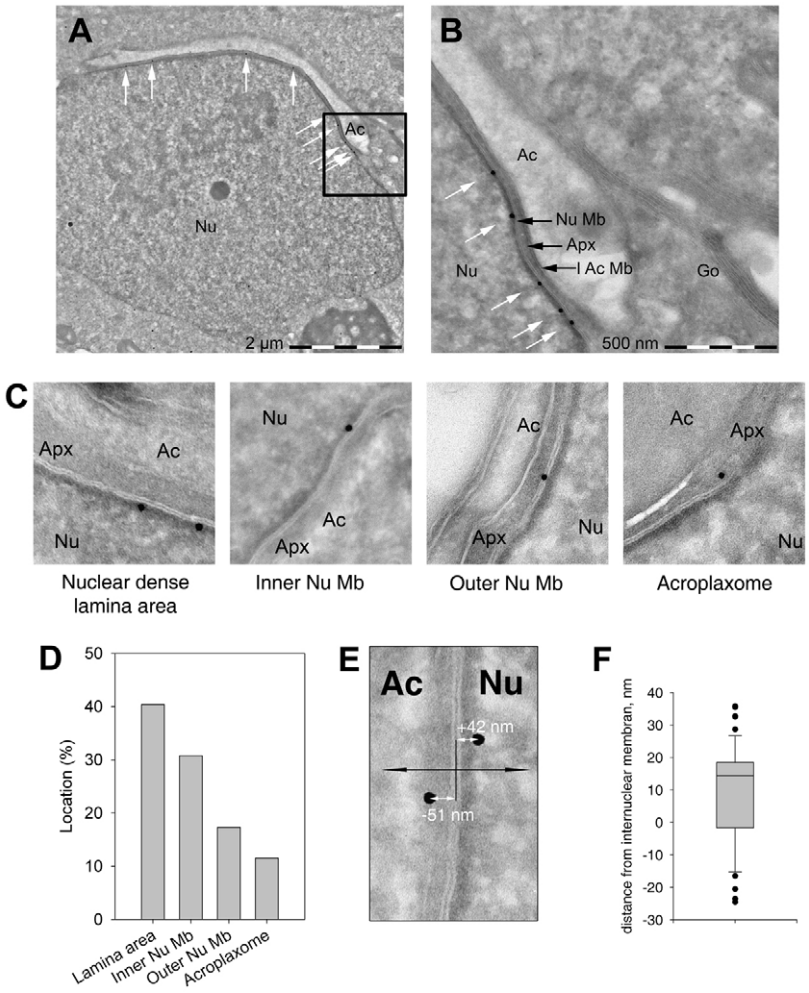

Fig. 4. Immunogold localization of Dpy19l2 in wild-type mouse spermatids. (**A**) Gold particles targeting Dpy19l2 antigenic sites were observed along the nuclear envelope of a spermatid in step 5/6 (white arrows). (**B**) Magnification of the black box drawn in A. (**C**) Representative localizations of gold particles at different locations. (**D**) Repartition of the gold particles in function of their localization, as presented in C. (**E**) Example of the measure of distances between the centre of the gold particle and the inter-nuclear membrane space. (**F**) Box plot showing the repartition of the numerical values of the distances measured for 52 gold particles. Nu, nucleus; Ac, acrosome; I Ac Mb, inner acrosomal membrane; Apx, acroplaxome; Nu Mb, nuclear membrane; Go, Golgi apparatus.

vesicles that cannot contribute to the normal acrosomal membrane spreading. Acrosome descent is unlikely to be due to vesicular traffic defects, as we did not measure any difference in the size of the Golgi apparatus or the number and size of Golgi-derived vesicles between wild-type and *Dpy19l2*$^{-/-}$ spermatids (data not shown). Surprisingly, in some spermatids corresponding to step 9, acrosome spreading progressed unilaterally and was thus defective (Fig. 6E,F). In addition, when observed at higher magnification, the bridging structure of spermatids at step 9 appeared discontinuous (Fig. 6F, inset).

The NDL facing the acrosome and the acroplaxome are defective in the absence of Dpy19l2

In Fig. 6B,F, the NDL facing the acrosome was partially missing and the thickness of the acroplaxome-lamina area structure was irregular in *Dpy19l2*$^{-/-}$ spermatids. In fact, the interaction between acroplaxome and NE seems to be dependent on the presence of the NDL: when it was present (Fig. 7A), the bridging structure allowing the interaction between acrosome and nucleus presented a normal layered structure and thickness. In its absence, the acroplaxome was loose and the thickness of the bridging structure was not uniform (Fig. 7A), contrary to the acroplaxome observed in wild-type spermatids (Fig. 7A, inset). At higher magnification, a swelling of the inter-nuclear membrane space was observed and NE membranes split off, the ONM remaining attached on the acroplaxome (Fig. 7B). The vanishing of the NDL led to a re-organization of the distribution of lamin B1: in wild-type round spermatids, lamin B1 is not present in the NE-facing acrosome and a strong polarization was observed with the acrosome at the anterior pole and lamin B1 at the posterior pole (supplementary material Fig. S5A,B). The absence of Dpy19l2 in deficient animals modifies the polarized distribution of lamin B1, which shifts to the anterior pole (supplementary material Fig. S5C,D). However, the vanishing of lamin B1 in elongated spermatids is not modified in *Dpy19l2*$^{-/-}$ spermatids (supplementary material Fig. S5E,F).

The disruption of the bridging structures leads to detachments of large parts of the acrosome from the nucleus (Fig. 8A-F). In tubule sections of *Dpy19l2*$^{-/-}$ animals, acrosomes were irregular and partially unbound to the nucleus (Fig. 8A,B). Acrosomes fully detached from the nucleus were also frequently observed (Fig. 8B). Acrosome fragmentation was observed from both partially elongated and non elongated acrosomes (Fig. 8C,D). Interestingly, the acroplaxome remained attached to the acrosome during detachment (Fig. 8C), indicating again that the rupture was due to a bridging defect between the acroplaxome and the NE. In more condensed spermatids, fully detached acrosomes with numerous vacuoles were observed in the cytoplasm (Fig. 8E). At later stages, no sp56 staining was observed in the vicinity of condensed nuclei, indicating that condensed spermatids were acrosomeless (Fig. 8F), suggesting that the detached acrosomes or acrosomal fragments were eliminated with the cytoplasmic components in the residual bodies during the last step of spermatid compaction.

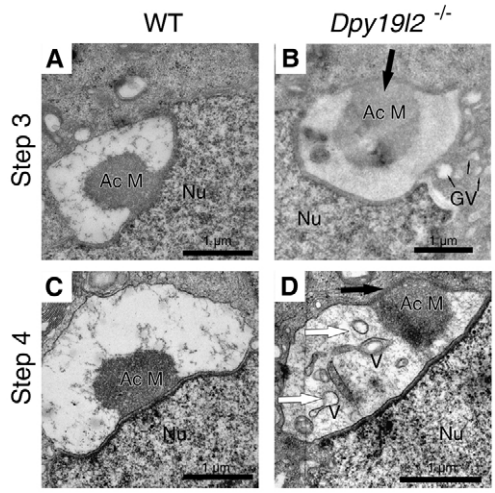

Fig. 5. Fine structure of acrosomes at step 3 and 4 of wild-type and *Dpy19l2*$^{-/-}$ spermatids. (A,C) Wild-type spermatids. (B,D) *Dpy19l2*$^{-/-}$ spermatids. (**A**) At step 3, the centre of the acrosomal matrix (Ac M) bound tightly to the nuclear membrane. (**B**) Large black arrow shows the ectopic localization of the acrosomal matrix in deficient spermatid. Small black arrows show fusing Golgi vesicles. (**C**) Ultrastructure of acrosome of a wild-type spermatid at step 4. (**D**) Similarly, ectopic acrosomal matrix was observed in *Dpy19l2*$^{-/-}$ spermatid at step 4. Moreover, vacuoles appeared within the acrosome (white arrows). Nu, nucleus; V, vacuole; GV Golgi vesicles.

Mislocalization of the manchette and of glycoproteins at the plasma membrane

During the spermatid elongation phase, a transient microtubular structure, known as the manchette, is implemented and is described as an important element of sperm morphogenesis. The manchette anchors on a perinuclear ring of actin associated with the marginal ring of the acroplaxome (Kierszenbaum et al., 2003). This microtubular structure is necessary for cargo traffic along the manchette and thus spermiogenesis (Zhou et al., 2009). In *Dpy19l2*$^{-/-}$ animals, condensed spermatids with round-nucleus, long microtubular structures corresponding to the manchette, were observed. However, they were not inserted around the nucleus but were free within the cell, contrary to wild-type spermatids (Fig. 9). In condensed spermatids from *Dpy19l2*$^{-/-}$ mice presenting a partial elongation, the manchette was longer than the nucleus and seemed anchored in the plasma membrane (Fig. 9C). Thus, the detachment of acrosome did not prevent manchette elongation but rather its anchoring at the right position. The manchette is important for proteins trafficking and its mislocalization may disturb protein distribution in spermatids (Kierszenbaum et al., 2011). Localization and dynamic of mouse sperm glycoproteins can be studied by lectin staining. *Pisum sativum* agglutinin (PSA) is a lectin widely used to visualize cell surface glycoproteins facing the acrosome. It has been shown that wild-type non-capacitated sperm present a typical PSA staining covering the dorsal and equatorial segments of the acrosome and the flagellum (Baker et al., 2004). Interestingly, globozoospermic sperm did not present any PSA staining in the head and in the flagellum (Fig. 9D), suggesting that glycoprotein trafficking is hampered during spermiogenesis of *Dpy19l2*$^{-/-}$ mice.

DISCUSSION

Acrosome biogenesis remains not fully characterized and, to date, there had been no protein described to link the acrosome to the nucleus (Kierszenbaum et al., 2011). This work suggests that DP19L2, as the first protein that anchors the acrosome to the nucleus, is likely to be central to a yet unexplored network of proteins that leads to the last steps of sperm differentiation. We demonstrate that Dpy19l2 is a transmembrane protein located in the INM and that its absence leads to the disruption of the layered structure present at the nuclear/acrosome junction during acrosome spreading and eventually to acroplaxome detachment from the nucleus.

In mammals DPY19L2 belongs to a family of four homologuous proteins: DPY19L1 to DPY19L4. This family does not present obvious homology with any other membrane proteins and clearly represents a new family of integral membrane proteins. In this paper, we characterized one of the members of this family and showed that Dpy19l2 is a membrane protein of the INM. As DPY19L2, DPY19L3 is also localized in the INM when expressed in cells lines. DPY19L proteins thus represent a new and original family of transmembrane proteins of the NE that are probably involved in nucleus/cytoplasm interactions.

Structure and function of Dpy19l2 protein in spermiogenesis

First, using different programs dedicated to transmembrane topology prediction (Sosui and Phobius), and comparing the results obtained first with transmembrane topology of Dpy19l2 in several

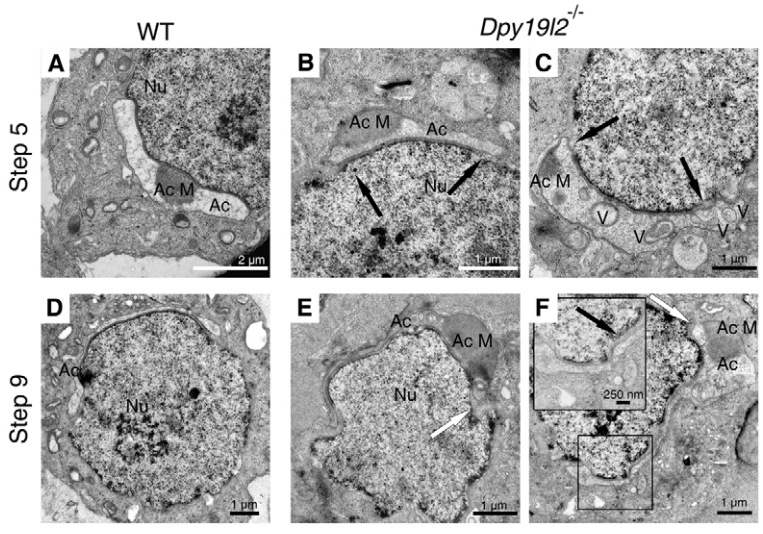

Fig. 6. Fine structure of acrosomes at step 5 and 9 of wild-type and *Dpy19l2*$^{-/-}$ spermatids. (A,D) Wild-type spermatids. (B,C,E,F) *Dpy19l2*$^{-/-}$ spermatids. (**A**) Step 5 of a wild-type spermatid showing the continuous nuclear dense lamina (NDL) following the acroplaxome. The vacuoles were absent and the acrosomal matrix was bound to the inner acrosomal membrane. (**B**,**C**) The NDL/acroplaxome layer was shortened and the acrosome extended widely beyond this structure (black arrows) in *Dpy19l2*$^{-/-}$ spermatids at step 5. The acrosomal matrix was localized ectopically and the NDL was discontinuous. (**D**) Step 9 of a wild-type spermatid showing the bilateral spread of the acrosome over the nucleus. The NDL/acroplaxome structures were continuous. (**E**,**F**) Unilateral spreading of acrosome in *Dpy19l2*$^{-/-}$ spermatids at step 9. The failure of contralateral spreading was indicated by white arrows. Disruptions of the NDL/acroplaxome structures were frequently observed (see black arrow in inset corresponding to the enlargement of the black box drawn in F). Ac, acrosome; Ac M, acrosomal matrix; Nu, nucleus; V, vacuole.

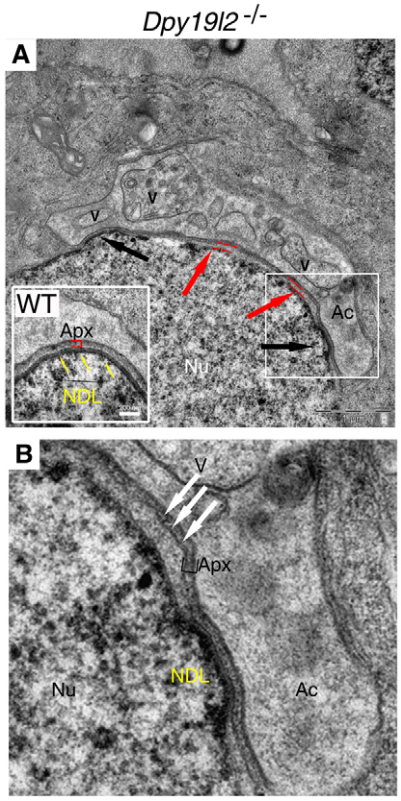

Fig. 7. The NDL is disrupted, acroplaxome comes loose and nuclear membranes split off in stage 8 *Dpy19l2*$^{-/-}$ spermatids. (**A**) Fine structure of the bridging structure between the acrosome and the nucleus in a *Dpy19l2*$^{-/-}$ mouse spermatid observed by EM. Acrosome (Ac) spread over the nucleus (Nu). Numerous vacuoles (V) were present in the lumen of the acrosome. Contrary to the wild-type bridging structure, where nuclear-dense lamina (NDL, yellow arrows) was continuous (inset), *Dpy19l2*$^{-/-}$ spermatid presented a disrupted NDL. Black arrows indicate where the NDL was still present. In the absence of the NDL, the acroplaxome (Apx) came loose (red arrows, red dashes indicate the detachment). (**B**) higher magnification of the boxed region in A. In the absence of the NDL, the INM and ONM were dissociated and the ONM remained attached to the acroplaxome (white arrows).

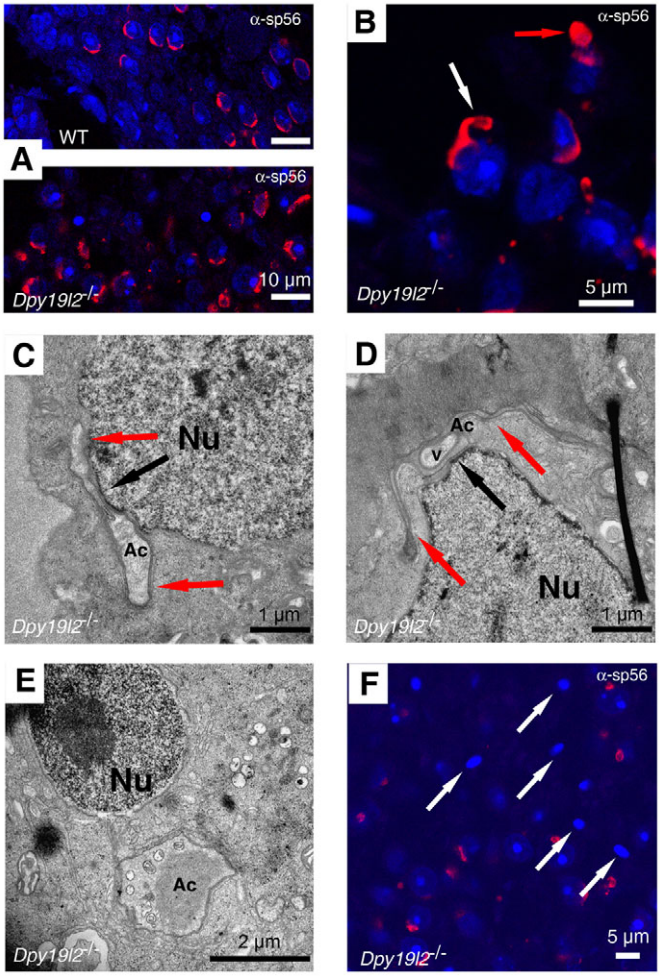

Fig. 8. Acrosome detachment during spermiogenesis in *Dpy19l2*$^{-/-}$ spermatids. (**A**) Confocal images of wild-type (up) and *Dpy19l2*$^{-/-}$ (down) testis tubule sections labeled with α-sp56 and Hoechst. The acroplaxome spread bilaterally and regularly in wild-type compared with *Dpy19l2*$^{-/-}$ spermatids. (**B**) At higher magnification, partially (white arrow) or fully (red arrow) detached acrosomes were observed. (**C**) Fine structure of a partially detached acrosome on the nucleus of a spermatid of step 5. The bridging structure was present only in the centre (black arrow) and both sides became loose (red arrows). (**D**) Similar detachment process in a spermatid at step 9: the bridging structure was almost completely disrupted and acrosome remained attached by a small area, where the NDL was conserved (black arrow). Red arrows show large parts of the acrosome detached from the nucleus. (**E**) In a more condensed spermatid, the acrosome was completely detached. Ac, Acrosome; Nu, nucleus; V, vacuole. (**F**) A tubule section of *Dpy19l2*$^{-/-}$ testis labeled with α-sp56: in fully condensed spermatids with round-shaped nucleus, the acrosome was no longer distinguishable (white arrows).

species (bovine, dog, mouse, human, pig and Chinese panda) and second with transmembrane topology of Dpy19l1, we estimated that Dpy19l2 is a transmembrane protein with 10 putative transmembrane segments (Fig. 10A). This model indicates the presence of two large N-terminal and C-terminal domains that will thus be located on the same side of the membrane. Second, immunogold labeling results unequivocally demonstrated that the N terminus of Dpy19l2 is located in the nucleoplasm (Fig. 4F) and immunostaining experiments performed on transfected cells (Fig. 3; supplementary material Fig. S3) demonstrated that the C terminus of DPY19L proteins is probably located in the nucleoplasm as well. Altogether, these results suggest that the N-terminal and C-terminal domains are located in the nucleoplasm. A putative topology of Dpy19l2 is presented in Fig. 10A.

The presence of Dpy19l2 does not seem to be necessary for acroplaxome and NDL positioning at step 3 and 4, suggesting that other proteins are involved during these phases. However, contrary to wild-type sperm, in *Dpy19l2*$^{-/-}$ sperm the acrosomal matrix is free within the acrosome and very often seems to be attached to the outer acrosomal membrane, suggesting that the bridging structure is in fact already defective. This bridging structure did not spread or was disrupted during the caudal descent of acrosome, suggesting that Dpy19l2 is required to stabilize the multi-layered structure challenged by forces applied during the elongation phase of the acrosome. The absence of Dpy19l2 lead to the disappearance of the NDL, then to multiple rupture points between both nuclear membranes or between NE and the acroplaxome, eventually

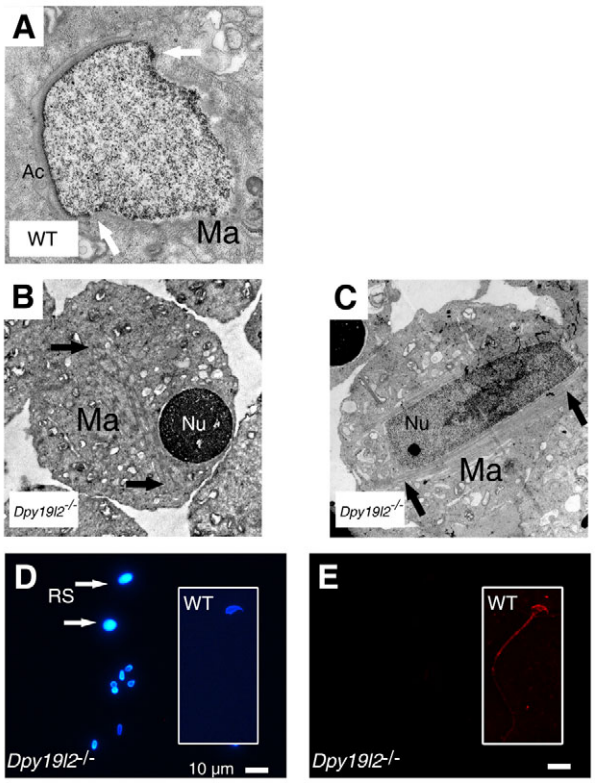

Fig. 9. The manchette is misplaced in *Dpy19l2*$^{-/-}$ spermatids. (**A**) In wild-type spermatid, manchette was attached to a structure located near the marginal zone of the acrosome (white arrows), corresponding to the marginal ring. (**B**,**C**) In *Dpy19l2*$^{-/-}$ spermatids, the manchette developed but did not anchor to the right location (black arrows) and seemed abnormally long. Nu, nucleus; Ac, Acrosome; Ma Manchette. (**D**,**E**) Epididymal sperm from *Dpy19l2*$^{-/-}$ males stained with Hoechst (D) and *Pisum sativum* agglutinin (PSA-rhodamin) (E). In D, there are two types of nuclei: small nuclei with a round or rod shape corresponding to globozoospermic sperm; and the nuclei of spermiogenesis-blocked spermatids (RS) presented in Fig. 1. Insets: Hoechst staining (blue) showing normal nucleus shape (arrows in D) and PSA staining (red) showing the distribution of glycoproteins in a wild-type sperm.

leading to acrosome detachment. The swelling of inter-nuclear membrane space followed by the separation of both nuclear membranes, have previously been documented in both human globozoospermia (Escalier, 1990) and mouse globozoospermia induced by the absence of casein kinase 2 (Escalier et al., 2003). Interestingly, as shown by EM, the acroplaxome remained attached to the acrosome during the detachment, thus confirming that Dpy19l2 is necessary to bridge the nucleus and the acroplaxome. The detachment of the acrosome removes the marginal ring of the acroplaxome and very likely prevents the adequate positioning of the perinuclear ring of the manchette. The manchette is thus mispositionned, leading to impaired intramanchette transport, sperm protein trafficking, and head and flagellum shaping (Kierszenbaum et al., 2011).

Our data clearly demonstrate that Dpy19l2 is involved in the preservation or stabilization of a specific NDL facing the acrosome. Lamin C2 and LAPs2 are not present in the postmeiotic phase and thus are unlikely partners of Dpy19l2 (Alsheimer et al., 1998). Lamin B1 and B3 are expressed during spermiogenesis, but their localizations are not compatible with the localization of Dpy19l2 in spermatids (Gob et al., 2010; Schutz et al., 2005). Interestingly, the absence of Dpy19l2 does not prevent the initial polarized organization of lamin B1, but the detachment of the acrosome leads to a reorganization of lamin B1, which shifts towards the anterior pole. This result suggests that the acrosome maintains a very specific NDL that remains uncharacterized.

A schematic drawing of the conclusions obtained from our studies is presented in Fig. 10B.

DPY19L as a functional partner of LINC complex

The localization of the nucleus within the cell changes during cell life and is accurately controlled mostly by SUN and KASH protein families (Burke and Roux, 2009; Tzur et al., 2006). Different SUN proteins are expressed during spermatogenesis and Sun proteins are thus likely to be involved in nuclear shaping during sperm head formation. Interestingly, Ima1, an integral transmembrane protein of the INM, has already been characterized in *S. pombe* and appears to functionally interact with SUN proteins. In the absence of Ima1, a partial dissociation of SUN-KASH complexes leads to nuclear membrane defects and lumen swelling, a phenotype also observed in *Dpy19l2*$^{-/-}$ spermatids (King et al., 2008). The mammalian ortholog of Ima1, Samp1, is also an INM protein and its absence leads to SUN1 mislocalization (Gudise et al., 2011). SUN interactions with proteins of the INM are thus central for their role as linker of nucleoskeleton and cytoskeleton. In this work, we have characterized a new family of proteins located in the INM, the absence of which leads to the disruption of the bridging structure required for acrosome attachment on the nucleus. Interestingly, Sun5, recently described in the NE facing the acrosome in mouse, shows a spatiotemporal pattern of expression very similar to that of Dpy19l2 (Frohnert et al., 2011). Our results show that SUN5 and DPY19L2 clustered in the NE in transfected HEK cells and partially colocalized. This suggests that SUN5 may be a structural partner of DPY19L2. The absence of Dpy19l2 may disrupt Sun5 function and thus acrosome binding. This model is, however, speculative as no knockout or knock-down of SUN5 has been presented so far to confirm this hypothesis. Very recently, it has been described that downregulation of Dpy19l1 and Dpy19l3 during neurogenesis of mouse embryos leads to strong migration anomalies of neurons (Watanabe et al., 2011), a phenotype similar to that observed for Sun/Kash LINC proteins knockdowns (Zhang et al., 2009). Dpy19l1/3 may be involved in Sun1/2 functioning in neuroblasts and this hypothesis could explain the striking similarity of Sun1/2 and Dpy19l1/3 deficiencies. The study of putative interactions between DPY19L proteins and conventional LINC complexes will be pursued.

Dpy19l2 knockout mice represents a good model for human globozoospermia

The prognosis for men diagnosed with globozoospermia remains very poor and treating globozoospermia represents a challenging task. This is surprising for a post-meiotic defect that does not affect chromosomal segregation (Dam et al., 2007a). However, several causes may explain this high rate of failure. For example, PLCζ, the sperm factor required for oocyte activation, is absent or minimally present in globozoospermia (Heytens et al., 2009; Taylor et al., 2010; Yoon et al., 2008). This compromises oocyte activation and therefore accounts, at least partly, for the low fertilization rate observed with these individuals.

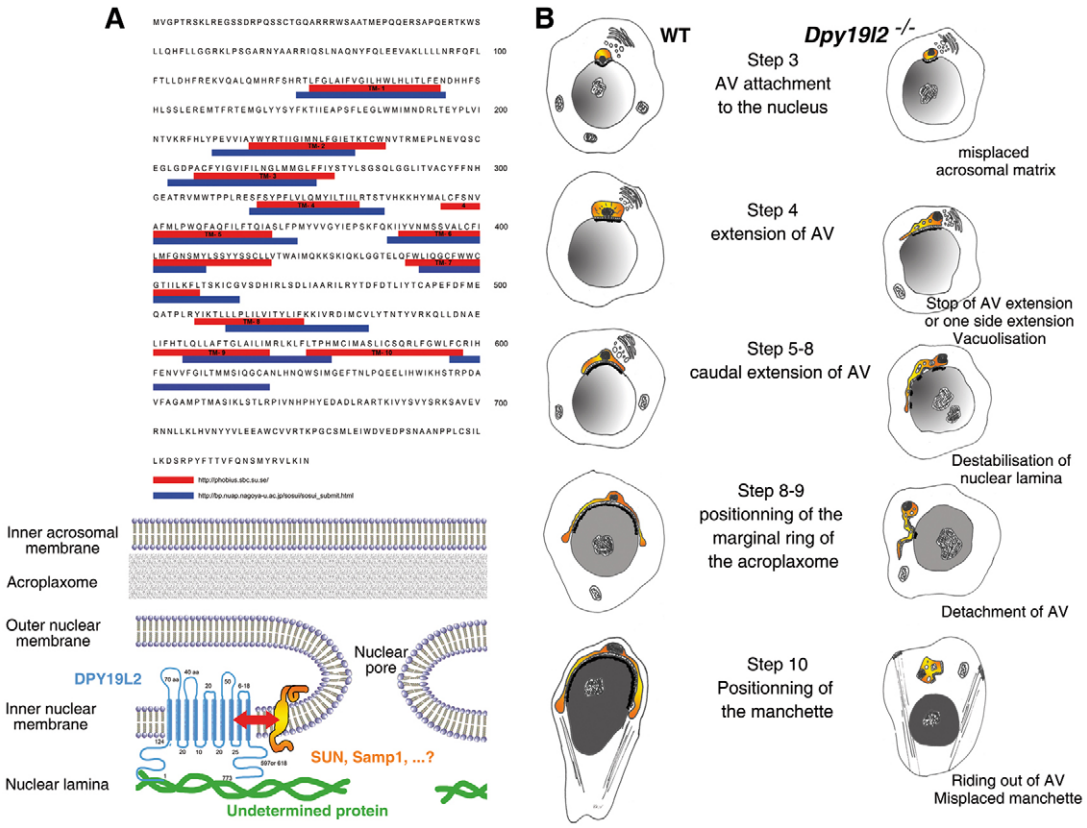

Fig. 10. Putative topology of Dpy19l2 and schematic description of spermiogenesis in *Dpy19l2*$^{-/-}$ spermatids. (**A**) Amino acid sequence analysis of Dpy19l2 with two different programs suggests that Dpy19l2 has 10 transmembrane domains. Dpy19l2 is located in the INM and several uncharacterized proteins, partners to Dpy19l2, are likely to be present in the NDL as well as in the INM and/or ONM in order to interconnect and regulate the interactions between the different layers. (**B**) The different steps of acrosome disruption in *Dpy19l2*$^{-/-}$ spermatids.

In order to understand the physiopathology of globozoospermia and the reasons for the treatment failure, a good animal model was sought for a long time. Contrary to the other mouse mutants described to present a similar phenotype and thus considered as models to understand human globozoospermia (supplementary material Table S1), our *Dpy19l2*$^{-/-}$ model exhibits all the characteristics of the human type 1 globozoospermia, including: (1) absence of the acrosome (Fig. 8F); (2) defects of nuclear shaping (Fig. 1), of the nuclear envelope (Fig. 7B) and of the acroplaxome (Fig. 6F); and (3) aberrant positioning of the manchette (Fig. 9). Moreover, in our model, *Dpy19l2*$^{-/-}$ spermatids presented a unique feature with NDL disruption leading to acroplaxome detachment from the nucleus. This defect was not observed in studies of several mouse globozoospermia described so far and performed by electron microscopy (supplementary material Table S1).

Because deletion of *DPY19L2* is the main cause of human globozoospermia (>70%), *Dpy19l2*$^{-/-}$ mice represent a perfect animal model with which to understand the physiopathology of globozoospermia and to investigate the causes of the low success rate observed in globozoospermic men treated by intra cytoplasmic sperm injection.

Acknowledgements
This work was supported by Le Centre national de la recherche scientifique (CNRS) (to C.A.), by the Agence Nationale de la Recherche (ANR Genopat 2009, projet ICG2I) (to V.P., C.A. and P.R.). We thank Denise Escalier, Annie Andrieux and Jacques Brocard for valuable discussions.

Competing interests statement
The authors declare no competing financial interests.

Supplementary material
Supplementary material available online at
http://dev.biologists.org/lookup/suppl/doi:10.1242/dev.077982/-/DC1

References
Alsheimer, M., Fecher, E. and Benavente, R. (1998). Nuclear envelope remodelling during rat spermiogenesis: distribution and expression pattern of LAP2/thymopoietins. *J. Cell Sci.* **111**, 2227-2234.
Audouard, C. and Christians, E. (2011). Hsp90beta1 knockout targeted to male germline: a mouse model for globozoospermia. *Fertil. Steril.* **95**, 1475-1477.
Baker, S. S., Thomas, M. and Thaler, C. D. (2004). Sperm membrane dynamics assessed by changes in lectin fluorescence before and after capacitation. *J. Androl.* **25**, 744-751.
Barcellona, W. J. and Meistrich, M. L. (1977). Ultrastructural integrity of mouse testicular cells separated by velocity sedimentation. *J. Reprod. Fertil.* **50**, 61-68.
Burke, B. and Roux, K. J. (2009). Nuclei take a position: managing nuclear location. *Dev. Cell* **17**, 587-597.
Carson, A. R., Cheung, J. and Scherer, S. W. (2006). Duplication and relocation of the functional DPY19L2 gene within low copy repeats. *BMC Genomics* **7**, 45.
Dahl, K. N., Kahn, S. M., Wilson, K. L. and Discher, D. E. (2004). The nuclear envelope lamina network has elasticity and a compressibility limit suggestive of a molecular shock absorber. *J. Cell Sci.* **117**, 4779-4786.
Dam, A. H., Feenstra, I., Westphal, J. R., Ramos, L., van Golde, R. J. and Kremer, J. A. (2007a). Globozoospermia revisited. *Hum. Reprod. Update* **13**, 63-75.
Dam, A. H., Koscinski, I., Kremer, J. A., Moutou, C., Jaeger, A. S., Oudakker, A. R., Tournaye, H., Charlet, N., Lagier-Tourenne, C., van Bokhoven, H. et al. (2007b). Homozygous mutation in SPATA16 is associated with male infertility in human globozoospermia. *Am. J. Hum. Genet.* **81**, 813-820.

Escalier, D. (1990). Failure of differentiation of the nuclear-perinuclear skeletal complex in the round-headed human spermatozoa. *Int. J. Dev. Biol.* **34**, 287-297.
Escalier, D., Silvius, D. and Xu, X. (2003). Spermatogenesis of mice lacking CK2alpha': failure of germ cell survival and characteristic modifications of the spermatid nucleus. *Mol. Reprod. Dev.* **66**, 190-201.
Frohnert, C., Schweizer, S. and Hoyer-Fender, S. (2011). SPAG4L/SPAG4L-2 are testis-specific SUN domain proteins restricted to the apical nuclear envelope of round spermatids facing the acrosome. *Mol. Hum. Reprod.* **17**, 207-218.
Gob, E., Schmitt, J., Benavente, R. and Alsheimer, M. (2010). Mammalian sperm head formation involves different polarization of two novel LINC complexes. *PLoS ONE* **5**, e12072.
Gudise, S., Figueroa, R. A., Lindberg, R., Larsson, V. and Hallberg, E. (2011). Samp1 is functionally associated with the LINC complex and A-type lamina networks. *J. Cell Sci.* **124**, 2077-2085.
Harbuz, R., Zouari, R., Pierre, V., Ben Khelifa, M., Kharouf, M., Coutton, C., Merdassi, G., Abada, F., Escoffier, J., Nikas, Y. et al. (2011). A recurrent deletion of DPY19L2 causes infertility in man by blocking sperm head elongation and acrosome formation. *Am. J. Hum. Genet.* **88**, 351-361.
Heytens, E., Parrington, J., Coward, K., Young, C., Lambrecht, S., Yoon, S. Y., Fissore, R. A., Hamer, R., Deane, C. M., Ruas, M. et al. (2009). Reduced amounts and abnormal forms of phospholipase C zeta (PLCzeta) in spermatozoa from infertile men. *Hum. Reprod.* **24**, 2417-2428.
Hodzic, D. M., Yeater, D. B., Bengtsson, L., Otto, H. and Stahl, P. D. (2004). Sun2 is a novel mammalian inner nuclear membrane protein. *J. Biol. Chem.* **279**, 25805-25812.
Honigberg, L. and Kenyon, C. (2000). Establishment of left/right asymmetry in neuroblast migration by UNC-40/DCC, UNC-73/Trio and DPY-19 proteins in C. elegans. *Development* **127**, 4655-4668.
Ito, C., Suzuki-Toyota, F., Maekawa, M., Toyama, Y., Yao, R., Noda, T. and Toshimori, K. (2004). Failure to assemble the peri-nuclear structures in GOPC deficient spermatids as found in round-headed spermatozoa. *Arch. Histol. Cytol.* **67**, 349-360.
Kang-Decker, N., Mantchev, G. T., Juneja, S. C., McNiven, M. A. and van Deursen, J. M. (2001). Lack of acrosome formation in Hrb-deficient mice. *Science* **294**, 1531-1533.
Kierszenbaum, A. L., Rivkin, E. and Tres, L. L. (2003). Acroplaxome, an F-actin-keratin-containing plate, anchors the acrosome to the nucleus during shaping of the spermatid head. *Mol. Biol. Cell* **14**, 4628-4640.
Kierszenbaum, A. L., Tres, L. L., Rivkin, E., Kang-Decker, N. and van Deursen, J. M. (2004). The acroplaxome is the docking site of Golgi-derived myosin Va/Rab27a/b- containing proacrosomal vesicles in wild-type and Hrb mutant mouse spermatids. *Biol. Reprod.* **70**, 1400-1410.
Kierszenbaum, A. L., Rivkin, E. and Tres, L. L. (2011). Cytoskeletal track selection during cargo transport in spermatids is relevant to male fertility. *Spermatogenesis* **1**, 221-230.
Kim, K. S., Cha, M. C. and Gerton, G. L. (2001). Mouse sperm protein sp56 is a component of the acrosomal matrix. *Biol. Reprod.* **64**, 36-43.
King, M. C., Drivas, T. G. and Blobel, G. (2008). A network of nuclear envelope membrane proteins linking centromeres to microtubules. *Cell* **134**, 427-438.
Koscinski, I., Elinati, E., Fossard, C., Redin, C., Muller, J., Velez de la Calle, J., Schmitt, F., Ben Khelifa, M., Ray, P. F., Kilani, Z. et al. (2011). DPY19L2 deletion as a major cause of globozoospermia. *Am. J. Hum. Genet.* **88**, 344-350.
Lin, Y. N., Roy, A., Yan, W., Burns, K. H. and Matzuk, M. M. (2007). Loss of zona pellucida binding proteins in the acrosomal matrix disrupts acrosome biogenesis and sperm morphogenesis. *Mol. Cell. Biol.* **27**, 6794-6805.
Liou, W., Geuze, H. J. and Slot, J. W. (1996). Improving structural integrity of cryosections for immunogold labeling. *Histochem. Cell Biol.* **106**, 41-58.
Lu, L., Lin, M., Xu, M., Zhou, Z. M. and Sha, J. H. (2006). Gene functional research using polyethylenimine-mediated in vivo gene transfection into mouse spermatogenic cells. *Asian J. Androl.* **8**, 53-59.
Mannowetz, N., Kartarius, S., Wennemuth, G. and Montenarh, M. (2010). Protein kinase CK2 and new binding partners during spermatogenesis. *Cell Mol. Life Sci.* **67**, 3905-3913.
Paiardi, C., Pasini, M. E., Gioria, M. and Berruti, G. (2011). Failure of acrosome formation and globozoospermia in the wobbler mouse, a Vps54 spontaneous recessive mutant. *Spermatogenesis* **1**, 52-62.
Romero, Y., Meikar, O., Papaioannou, M. D., Conne, B., Grey, C., Weier, M., Pralong, F., De Massy, B., Kaessmann, H., Vassalli, J. D. et al. (2011). Dicer1 depletion in male germ cells leads to infertility due to cumulative meiotic and spermiogenic defects. *PLoS ONE* **6,** e25241.
Romrell, L. J., Bellve, A. R. and Fawcett, D. W. (1976). Separation of mouse spermatogenic cells by sedimentation velocity. A morphological characterization. *Dev. Biol.* **49**, 119-131.
Schirren, C. G., Holstein, A. F. and Schirren, C. (1971). Uber die Morphogenese rundkopfiger Spermatozoen des Menschen. *Andrologie* **3**, 117-125.
Schutz, W., Alsheimer, M., Ollinger, R. and Benavente, R. (2005). Nuclear envelope remodeling during mouse spermiogenesis: postmeiotic expression and redistribution of germline lamin B3. *Exp. Cell Res.* **307**, 285-291.
Tang, T., Li, L., Tang, J., Li, Y., Lin, W. Y., Martin, F., Grant, D., Solloway, M., Parker, L., Ye, W. et al. (2010). A mouse knockout library for secreted and transmembrane proteins. *Nat. Biotechnol.* **28**, 749-755.
Taylor, S. L., Yoon, S. Y., Morshedi, M. S., Lacey, D. R., Jellerette, T., Fissore, R. A. and Oehninger, S. (2010). Complete globozoospermia associated with PLCzeta deficiency treated with calcium ionophore and ICSI results in pregnancy. *Reprod. Biomed. Online* **20**, 559-564.
Tzur, Y. B., Wilson, K. L. and Gruenbaum, Y. (2006). SUN-domain proteins: 'Velcro' that links the nucleoskeleton to the cytoskeleton. *Nat. Rev. Mol. Cell Biol.* **7**, 782-788.
Walden, C. M., Sandhoff, R., Chuang, C. C., Yildiz, Y., Butters, T. D., Dwek, R. A., Platt, F. M. and van der Spoel, A. C. (2007). Accumulation of glucosylceramide in murine testis, caused by inhibition of beta-glucosidase **2**, implications for spermatogenesis. *J. Biol. Chem.* **282**, 32655-32664.
Watanabe, K., Takebayashi, H., Bepari, A. K., Esumi, S., Yanagawa, Y. and Tamamaki, N. (2011). Dpy19l1, a multi-transmembrane protein, regulates the radial migration of glutamatergic neurons in the developing cerebral cortex. *Development* **138**, 4979-4990.
Xiao, N., Kam, C., Shen, C., Jin, W., Wang, J., Lee, K. M., Jiang, L. and Xia, J. (2009). PICK1 deficiency causes male infertility in mice by disrupting acrosome formation. *J. Clin. Invest.* **119**, 802-812.
Xu, X., Toselli, P. A., Russell, L. D. and Seldin, D. C. (1999). Globozoospermia in mice lacking the casein kinase II alpha' catalytic subunit. *Nat. Genet.* **23**, 118-121.
Xu, M., Xiao, J., Chen, J., Li, J., Yin, L., Zhu, H., Zhou, Z. and Sha, J. (2003). Identification and characterization of a novel human testis-specific Golgi protein, NYD-SP12. *Mol. Hum. Reprod.* **9**, 9-17.
Yao, R., Ito, C., Natsume, Y., Sugitani, Y., Yamanaka, H., Kuretake, S., Yanagida, K., Sato, A., Toshimori, K. and Noda, T. (2002). Lack of acrosome formation in mice lacking a Golgi protein, GOPC. *Proc. Natl. Acad. Sci. USA* **99**, 11211-11216.
Yatsenko, A. N., O'Neil, D. S., Roy, A., Arias-Mendoza, P. A., Chen, R., Murthy, L. J., Lamb, D. J. and Matzuk, M. M. (2011). Association of mutations in the zona pellucida binding protein 1 (ZPBP1) gene with abnormal sperm head morphology in infertile men. *Mol. Hum. Reprod.* **18**, 14-21.
Yildiz, Y., Matern, H., Thompson, B., Allegood, J. C., Warren, R. L., Ramirez, D. M., Hammer, R. E., Hamra, F. K., Matern, S. and Russell, D. W. (2006). Mutation of beta-glucosidase 2 causes glycolipid storage disease and impaired male fertility. *J. Clin. Invest.* **116**, 2985-2994.
Yoon, S. Y., Jellerette, T., Salicioni, A. M., Lee, H. C., Yoo, M. S., Coward, K., Parrington, J., Grow, D., Cibelli, J. B., Visconti, P. E. et al. (2008). Human sperm devoid of PLC, zeta 1 fail to induce Ca(2+) release and are unable to initiate the first step of embryo development. *J. Clin. Invest.* **118**, 3671-3681.
Zhang, X., Lei, K., Yuan, X., Wu, X., Zhuang, Y., Xu, T., Xu, R. and Han, M. (2009). SUN1/2 and Syne/Nesprin-1/2 complexes connect centrosome to the nucleus during neurogenesis and neuronal migration in mice. *Neuron* **64**, 173-187.
Zhong, Z., Wilson, K. L. and Dahl, K. N. (2010). Beyond lamins: other structural components of the nucleoskeleton. *Methods Cell Biol.* **98**, 97-119.
Zhou, J., Du, Y. R., Qin, W. H., Hu, Y. G., Huang, Y. N., Bao, L., Han, D., Mansouri, A. and Xu, G. L. (2009). RIM-BP3 is a manchette-associated protein